Colloids and Surfaces B: Biointerfaces 132 (2015) 290–298

Contents lists available at ScienceDirect

Colloids and Surfaces B: Biointerfaces

journal homepage: www.elsevier.com/locate/colsurfb

Rhamnolipids functionalized AgNPs-induced oxidative stress and modulation of toxicity pathway genes in cultured MCF-7 cells

Sourabh Dwivedi[a], Quaiser Saquib[b], Abdulaziz A. Al-Khedhairy[b], Javed Ahmad[b], Maqsood A. Siddiqui[b], Javed Musarrat[a,*]

[a] Department of Agricultural Microbiology, Faculty of Agricultural Sciences, Aligarh Muslim University, Aligarh 202002, U.P., India
[b] Chair for DNA Research, Department of Zoology, College of Science, King Saud University, P.O. Box 2455, Riyadh 11451, Saudi Arabia

ARTICLE INFO

Article history:
Received 28 January 2015
Received in revised form 23 April 2015
Accepted 18 May 2015
Available online 27 May 2015

Keywords:
Rhamnolipid
ROS
Cytotoxicity
Gene expression
Silver nanoparticles
XRD

ABSTRACT

Rhamnolipids extracted from *Pseudomonas aeruginosa* strain JS-11 were utilized for synthesis of stable silver nanoparticles (Rh-AgNPs). The Rh-AgNPs (23 nm) were characterized by Fourier transform infrared (FTIR) spectroscopy, atomic force microscopy (AFM) and transmission electron microscopy (TEM). The cytotoxicity assays suggested significant decrease in viability of Rh-AgNPs treated human breast adenocarcinoma (MCF-7) cells, compared with normal human peripheral blood mononuclear (PBMN) cells. Flow cytometry data revealed 1.25-fold ($p < 0.05$) increase in the fluorescence of 2′,7′-dichlorofluorescein (DCF) at 0.25 μg/mL. However, at Rh-AgNPs concentrations of 0.5 and 1.0 μg/mL, much lesser fluorescence was noticed, which is attributed to cell death. Results with the fluorescent probe Rh123 demonstrated change in inner mitochondrial membrane and dissipation of membrane potential. The cell cycle analysis suggested 19.9% ($p < 0.05$) increase in sub-G1 peak with concomitant reduction in G1 phase at 1 μg/mL of Rh-AgNPs, compared to 2.7% in untreated control. The real-time RT^2 Profiler^{TM} PCR array data elucidated the overexpression of seven oxidative stress and DNA damage pathways genes viz. BAX, BCl_2, Cyclin D1, DNAJA1, E2F transcription factor 1, GPX1 and HSPA4, associated with apoptosis signaling, proliferation and carcinogenesis, pro inflammatory and heat shock responses in Rh-AgNPs treated cells. Thus, the increased ROS production, mitochondrial damage and appearance of sub-G1 (apoptotic) population suggested the anti-proliferative activity, and role of oxidative stress pathway genes in Rh-AgNPs induced death of MCF-7 cancer cells.

1. Introduction

Development of a reliable, eco-friendly and toxicity-free synthesis of metal nanoparticles (NPs) is an important aspect of nanotechnology research [1]. Lately, the biomimetic and green synthesis of AgNPs using polymer matrices such as starch [2], chitosan [3], cyclodextrins [4], and microbial biomass [5–7] has been extensively pursued. Microbial synthesis of NPs yields stable particles due to protein capping and interaction with other reducing agents such as nitrate reductase [8], naphthoquinones [9], and anthraquinones [10], secreted by the organisms. Furthermore, synthetic chemicals such as amine and carboxylate surfactants [11], cationic cetylpyridinium, or anionic sodium dodecyl sulphate, or non-ionic Brij 56 [12] have also been used for NPs synthesis. These surfactants are tension-active molecules, amphipathic in nature with both hydrophilic and hydrophobic moieties, and exhibit surface-active properties. With the increasing demand for greener bioprocesses and novel enhancers for NPs synthesis, the biosurfactants, and/or biosurfactant producing microbes are emerging as an alternate source. Thus, biosurfactants with the high surface activity and low critical micelle concentrations (CMC) are regarded as promising substitutes for synthetic surfactants [13]. Several microorganisms like bacteria, fungi, yeasts, and algae are good sources of biosurfactants and offer many advantages over their chemical counterparts. Therefore, the biosurfactant mediated synthesis of NPs is regarded as a clean, non-toxic, and environmentally acceptable "green chemistry" procedure, resulting in reduced NPs aggregation and uniform morphology. Furthermore, the lower toxicity, higher biodegradability, better environmental compatibility, higher foaming, high selectivity and specific activity at extreme temperatures, pH, and salinity [14] are some added advantages over the chemical surfactants.

In this context, the natural rhamnolipids, a subclass of glycolipids produced by bacteria, could serve as simple and economical

* Corresponding author. Tel.: +91 9760785651.
E-mail address: musarratj1@yahoo.com (J. Musarrat).

http://dx.doi.org/10.1016/j.colsurfb.2015.05.034
0927-7765/

stabilizer for AgNPs synthesis. Rhamnolipids from *Pseudomonas aeruginosa* strain BS-161R and its mutant EBN-8 have earlier been used for synthesis of silver NPs (AgNPs) in reverse micelles and composite rhamnolipids-gold NPs microtubules [15,16]. *Pseudomonas* species are well known for their capability to produce rhamnolipid biosurfactants on different carbon sources [17,18]. This has prompted us to develop a simple one-pot method for synthesis of highly stable and dispersible Rh-AgNPs. In this study, we report the role of natural rhamnolipids extracted from the culture supernatant of *P. aeruginosa* strain JS-11, as a stabilizing agent in synthesis of AgNPs. The synthesized Rh-AgNPs were characterized using the analytical techniques, viz., UV-visible spectrophotometry, XRD spectroscopy, TEM, FTIR and AFM. Rh-AgNPs induced antiproliferative activity and involvement of oxidative stress and toxicity pathways genes have been investigated in human breast adenocarcinoma (MCF7) cells, as an in vitro model.

2. Materials and methods

2.1. Bacterial strain characterization and screening for rhamnolipid production

The soil bacteria *P. aeruginosa* strain JS-11 has been obtained from culture collection of our laboratory [19]. The strain JS-11 was screened for rhamnolipids biosynthesis using the mineral salt-CTAB-methylene blue agar plates, following the method of Inka and Fritz [20]. Briefly, the cell-free culture supernatant (30 μL) was loaded into each pre-cut wells in methylene blue agar plate. The plate was then incubated at 37 °C for 72 h. A dark blue halo zone around the culture was considered as positive for anionic biosurfactant production.

2.2. Extraction of rhamnolipid produced by P. aeruginosa JS-11 in culture medium

For isolation of rhamnolipids, the culture of JS-11 was grown in a mineral salt medium containing (g/L); 15 g $NaNO_3$, 1.1 g KCl, 1.1 g NaCl, 0.00028 g $FeSO_4{\cdot}7H_2O$, 3.4 g KH_2PO_4, 4.4 g K_2HPO_4, 0.5 g $MgSO_4{\cdot}7H_2O$, 0.5 g yeast extract and 40 g glucose at 37 °C in a shaker incubator. Rhamnolipids released by the cells in culture medium were recovered by separating the cells from culture supernatant by centrifugation at 10,000 rpm. The supernatant was then acidified using hydrochloric acid to obtain pH 2.0. The precipitated rhamnolipids were collected by centrifugation at 10,000 rpm. The precipitate was suspended in 0.5 mL Milli Q water and extracted with 1 mL chloroform: ethanol (2:1, v/v). The extract was evaporated to near dryness and a reasonably pure rhamnolipids obtained. The surface tension of the crude rhamnolipids preparation was measured by the Wilhelmy plate method with a Du-Nouy tensiometer (K100MK2 Processor Tensiometer; Krüss, Hamburg, Germany). The critical micelle concentration (CMC) was determined by method of Sheppard and Mulligan [21].

2.3. Synthesis of rhamnolipids stabilized AgNPs

The Rh-AgNPs composite was prepared by mixing 10 mL of 1 mM $AgNO_3$ solution with 100 μL of rhamnolipids extract under vigorous stirring for 1 h at 30 °C. Subsequently, 2 mL of 5 mM $NaBH_4$ solution was added under constant stirring to obtain a red colored solution. The Rh-AgNPs were freeze-dried on a lyophilizer (Heto-Holten, Denmark) and stored in lyophilized powdered form, until used for further characterization.

2.4. Characterization of Rh-AgNPs

2.4.1. UV–vis spectral analysis

Change in the color intensity of the Rh-AgNPs with increasing time was measured after 2, 24, 48 and 72 h of incubation at 30 °C. For stability determination, the spectral measurements were performed up to 180 days. The spectra of the surface plasmon resonance (SPR) of Rh-AgNPs were recorded by use of a UV–vis spectrophotometer Cintra 10e GBC (Victoria, Australia) in wavelength range of 200–800 nm.

2.4.2. X ray diffraction analysis

The finely powdered freeze-dried sample of Rh-AgNPs was analyzed by X-ray powder diffractometer (PANalytical X'pert PRO, USA) using CuK_α radiation ($\lambda = 1.54056$ Å) in the range of $20° \leq 2\theta \leq 80°$ at 40 keV. The particle size (D) of the sample was estimated from the line width of the (1 1 1) XRD peak based on Scherrer's relationship ($D = 0.9\lambda/\beta\cos\theta$) [22], where λ is the wavelength of X-ray, β is the broadening of the diffraction line measured half of its maximum intensity in radians and θ is the Bragg's diffraction angle.

2.4.3. Transmission electron microscopic (TEM) analysis

Transmission electron micrographs were obtained on FEI Morgagni™ 268 (D) instrument (Italy) with an accelerating voltage of 80 kV. Samples for TEM analysis were prepared by drop-coating of Rh-AgNPs solution onto carbon-coated copper TEM grids. The films on the TEM grids were allowed to stand for 2 min, followed by removal of excess solution using a blotting paper, and the grid dried prior to observations.

2.4.4. Atomic force microscopic (AFM) analysis

Rh-AgNPs were examined using Innova AFM (Veeco Instruments, Plainview, NY, USA) in a non-contact tapping mode. The topographical images were obtained in tapping mode at a resonance frequency of 218 kHz. Tapping mode imaging was implemented in ambient air by oscillating the cantilever assembly at or near the cantilever's resonant frequency using a piezoelectric crystal. Characterization was done by observing the patterns on the surface topography and data analysis through WSXM software.

2.4.5. Infrared spectroscopic studies

Fourier transform infrared spectroscopy (FTIR) was performed for examining the functional groups of the rhamnolipids extracted from strain JS-11 culture by use of Interspec 2020 FTIR (SPECTROLAB U.K.). Briefly, the lyophilized Rh-AgNPs powder was mixed with spectroscopic grade potassium bromide (KBr) in the ratio of 1:100 and spectrum recorded in the range of 400–4000 wavenumber (cm^{-1}) on Interspec 2020 FTIR in the diffuse reflectance mode at a resolution of 4 cm^{-1} in KBr pellets. The spectrum of rhamnolipids associated with Rh-AgNPs was compared with the published spectrum of pure rhamnolipids available in scientific literature [23].

2.5. Cell culture and exposure to Rh-AgNPs

Human breast adenocarcinoma (MCF-7) cell line was used to examine the cytotoxicity of the Rh-AgNPs. The MCF-7 cells were obtained from the American Type Culture Collection (ATCC) (Manassas, VA). The cells showing more than 95% cell viability and passage number between 16 and 18 were used in the present study. Cells were cultured in DMEM/F-12 medium supplemented with 10% FBS and 100 U/mL penicillin–streptomycin at 5% CO_2 and 37 °C. At 85% confluence, cells were harvested using 0.25% trypsin and were sub-cultured in 6-well plates. Cells were allowed to attach on the surface for 24 h prior to treatment. Rh-AgNPs were suspended in cell culture medium and diluted to appropriate concentrations

(0.1, 0.2, 0.5, 1, 2, 5 and 10 μg/mL). The appropriate dilution of Rh-AgNPs were then sonicated at room temperature for 10 min at 40 W to avoid NPs aggregation prior to administration to cells. After treatment, the cells were harvested to determine the cell viability, membrane integrity and intracellular ROS generation as cytotoxicity end points. Human peripheral blood mononuclear (PBMN) cells and untreated MCF-7 cells were used as controls, under identical conditions.

2.5.1. Isolation of human PBMN cells

Human PBMN cells were obtained following the method described by Musarrat et al. [24]. Briefly, 3 mL blood was drawn through venous puncture and added to 3 mL of RPMI 1640. It was layered over 2 mL of histopaque 1077 and centrifuged at 800 × *g* for 20 min. The visible layer of lymphocytes formed at the media-histopaque interface was carefully aspirated. The lymphocytes were rinsed with RPMI by centrifugation at 250 × *g* for 10 min. The recovered pellet was resuspended in RPMI medium and processed for experiments.

2.5.2. Tetrazolium bromide salt (MTT) and Neutral red uptake (NRU) assays

The viability of MCF-7 cells was assessed by 3-(4,5-dimethylthiazol-2-yl)-2,5-diphenyltetrazolium bromide (MTT) assay, as described by Dwivedi et al. [25]. The NRU assay was carried out following the protocol, described by Siddiqui et al. [26]. Parallel controls were run under identical conditions.

2.6. Zeta potential measurements

The Zeta potential of Rh-AgNPs was determined by use of a Zeta Potential Analyzer (Malvern Instruments Corporation, UK). Measurements were recorded at 25 °C suspended in PBS (pH 7.4) with an Ag electrode using phase analysis light scattering mode.

2.7. Measurement of mitochondrial membrane potential ($\Delta\Psi m$)

Flow cytometric measurements of ΔΨm of Rh-AgNPs treated MCF-7 cells were performed with a fluorescent dye Rh123, as described earlier [25]. In brief, the cells treated with 0.25, 0.5 and 1 μg/mL of Rh-AgNPs for 3 h were harvested and centrifuged at 1000 rpm for 4 min. Pellets were resuspended in 500 μL of PBS containing mitochondrial specific fluorescence dye Rh123 (5 μg/mL) for 60 min at 37 °C in dark. The cells were immediately washed twice with 1X PBS at 1000 rpm for 5 min at room temperature and pellets were resuspended in 500 μL of 1X PBS. ΔΨm was measured by use of flow cytometry and expressed as the mean fluorescence intensity (MnXI) of 10,000 cells.

2.8. Detection of intracellular reactive oxygen species by flow cytometry

Intracellular ROS were analyzed by flow cytometry using 2′,7′-dichloro dihydro fluorescein diacetate (DCFH-DA; Sigma–Aldrich), as a specific dye probe, which fluoresces on oxidation by reactive oxygen species to 2′,7′-dichlorofluorescein (DCF), following the method of Dwivedi et al. [25]. In brief, MCF-7 cells treated with 0.25, 0.5 and 1 μg/mL of Rh-AgNPs for 3 h were harvested and centrifuged at 1000 rpm for 4 min. Pellets were suspended in 500 μL of 1X PBS containing DCFH-DA (5 μM in DMSO) and incubated for 60 min at 37 °C in dark. Cells were then washed and resuspended in 500 μL 1X PBS. The fluorescence of cells (10,000 cells each) was recorded under 488 nm excitation. Green fluorescence from DCF was measured in the FL1 Log channel through a 525-nm band-pass filter on a flow cytometer Coulter EPICS XL-MCL (Beckman Coulter Company, Miami, FL, USA).

2.9. Flow cytometric analysis of cell cycle progression and apoptosis/necrosis

MCF-7 cells treated with 0.25, 0.5 and 1 μg/mL of Rh-AgNPs for 3 h were harvested and centrifuged at 1000 rpm for 4 min. Cells treated with 0.1% DMSO were used as a solvent control. Pellets were resuspended in 500 μL of 1X PBS. Cells were fixed with equal volume of chilled 70% ice-cold ethanol, and incubated at 4 °C for 1 h. After two successive washes with PBS at 1000 rpm for 4 min, cell pellets were resuspended in PBS, and stained with 50 μg/mL propidium iodide (PI) containing 0.1% Triton X-100 and 0.5 mg/mL RNAase A for 1 h at 30 °C in dark. Fluorescence of the PI was measured by use of a Beckman Coulter flow cytometer through FL-4 filter (585 nm) and 10,000 events were acquired. The data were analyzed by Coulter Epics XL-MCL, System II Software, Version 3.0. Cell debris characterized by a low FSC/SSC was excluded from the analysis.

2.10. Rh-AgNPs induced transcriptional analysis by quantitative real-time (RT)-PCR array

Relative gene expression of 84 genes responsible for human stress and toxicity pathway were quantified using RT^2 Profiler ™PCR Array (Cat. no. PAHS-003 A; SA Biosciences Corporation, Frederick, MD, USA) in a 96-well array format, following 24 h exposure of MCF-7 cells to 1 μg/mL of Rh-AgNPs. cDNA equivalent to 1 μg of total RNA was used for each array. The arrays were run on Roche® LightCycler® 480 (96-well block) (Rotkreuz, Switzerland) following the recommended cycling programs. Expression data obtained with Rh-AgNPs treatment group were normalized to the average Ct value of five housekeeping genes (*B2M, HPRT1, RPL13A, GAPDH* and *ACTB*) and expressed with respect to the untreated control. RT-PCR array data were evaluated from at least three independent experiments. The resultant ΔCt values were combined to calculate the average fold regulation values. Genes that were significantly different for Rh-AgNPs vs. the control were determined by a Student's *t*-test ($p < 0.05$) comparing the ΔCt values for the triplicate trials for each test sample with the ΔCt values for the control. Data expressed as mean ± SD for the values obtained from at least three independent experiments. Statistical analysis was performed by one-way analysis of variance (ANOVA) using Dunnett's multiple comparison test (Sigma Plot 11.0, USA). The level of statistical significance chosen was $p < 0.05$, unless otherwise stated.

3. Results and discussion

3.1. Synthesis and stability of Rh-AgNPs

The rhamnolipids released by *P. aeruginosa* strain JS-11 in LB and mineral salt medium containing 4% glucose resulted in decreased surface tension of the medium from 69 mN m^{-1} to 31 mN m^{-1}, which confirms the presence of biosurfactant in the culture medium. This corroborates with the observations of Rahman et al. [27]. The concentration of the extracted rhamnolipids from the strain JS-11 was determined to be 325 mg/L. The rhamnolipids emulsion in Milli Q water (Supplementary Fig. 1) has been used as a stabilizer at a very low (non-toxic) concentration of 0.005%, during synthesis of Rh-AgNPs. The color of the reaction mixture changed from colorless to yellowish-brown (Supplementary Fig. 1). The change in color was due to collective oscillation of the conduction electrons of the AgNPs produced in the reaction mixture, which increased significantly with time of exposure up to 72 h. The spectrum in Fig. 1 shows a characteristic band at 420 nm

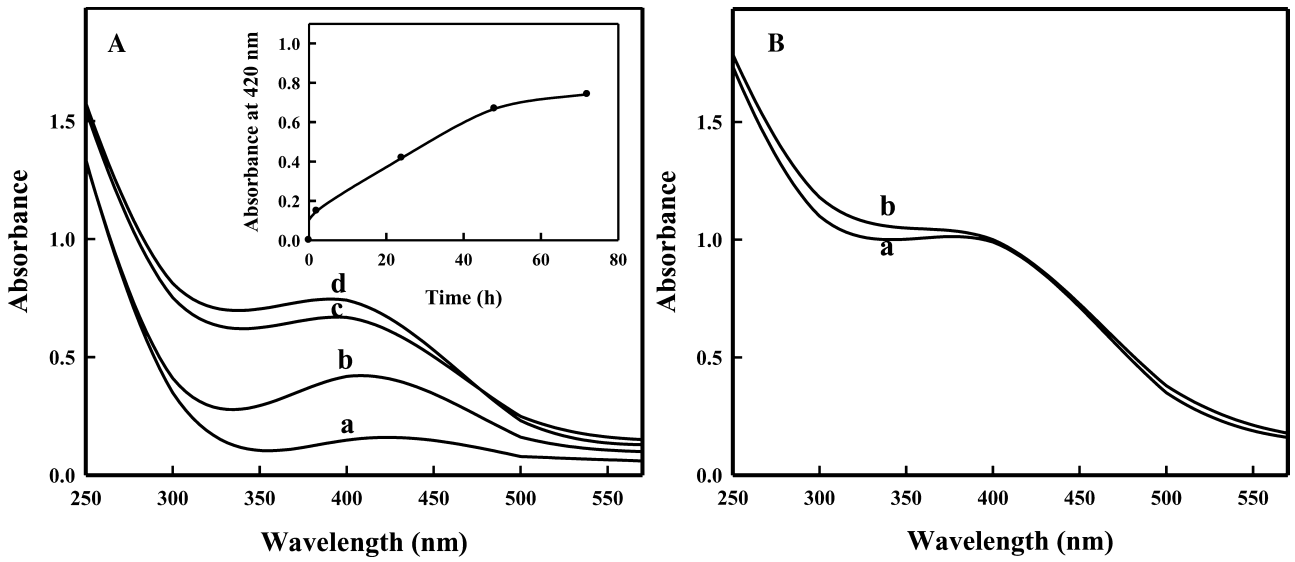

Fig. 1. UV–visible absorption spectra of Rh-AgNPs. (A) The change in absorbance with time during synthesis of Rh-AgNPs. The alphabets represent as (a) 2 h, (b) 24 h, (c) 48 h, (d) 72 h of incubation. The inset shows the change in SPR as a function of time. (B) The stability of Rh-AgNPs in suspension. The alphabets represent absorbance as (a) after 7 days, and (b) 180 days of incubation.

by reduction of the aqueous metal ions, suggesting the synthesis of AgNPs. The increase in SPR with incubation time up to 72 h might have occurred due to gradual reduction of $AgNO_3$ in presence of rhamnolipids. Most likely, the addition of rhamnolipids to $AgNO_3$ solution prior to $NaBH_4$ reduction, under our experimental conditions, may form a corona (capping) surrounding the Ag ions, which results in slow reduction. It is well known that colloidal AgNPs exhibit absorption at the wavelength from 390 to 420 nm due to Mie scattering [28]. Hence, the band at 420 nm can be attributed to the property of Mie scattering. Also, the plasmon band has been symmetric, which indicates that the solution does not contain much of aggregated particles. Further, no absorption peak corresponding to the control supernatant or silver ion solution was observed in the range of measurement. The Rh-AgNPs were quite stable as no significant change in the absorbance of the colloidal AgNPs solution occurred up to 180 days. The comparative spectra in Fig. 1B demonstrate the prolonged stability of Rh-AgNPs. The results elucidate that the rhamnolipids in the reaction milieu act as capping agent and stabilize the AgNPs by developing steric hindrance around the particles, which prevents aggregation of the NPs due to electrostatic interactions.

Supplementary Fig. S1 related to this article can be found, in the online version, at http://dx.doi.org/10.1016/j.colsurfb.2015.05.034

3.2. Physical attributes and stability of AgNPs

The XRD pattern obtained for the Rh-AgNPs shows four intense peaks in the whole spectrum of 2θ values ranging from 20 to 80. The diffractions at 38°, 44.18°, 64.29° and 77.19° can be indexed to the (1 1 1), (2 0 0), (2 2 0) and (3 1 1) planes of the face-centered cubic (fcc) silver, respectively (Fig. 2). The pattern clearly suggests that the Rh-AgNPs formed by the reduction of Ag^+ ions are crystalline in nature. The lattice parameters calculated by the Powder X software revealed that the maximum deviation that occurred between the observed and calculated values of interplanar spacing (d) remains below 0.002 Å. The full-width-at-half-maximum (FWHM) values measured for 1 1 1, 2 0 0, 2 2 0, and 3 1 1 planes of reflection were used to calculate the size of the NPs. The calculated average particle size of the Rh-AgNPs was determined to be 23 nm, which has been found to be in size range obtained through TEM analysis.

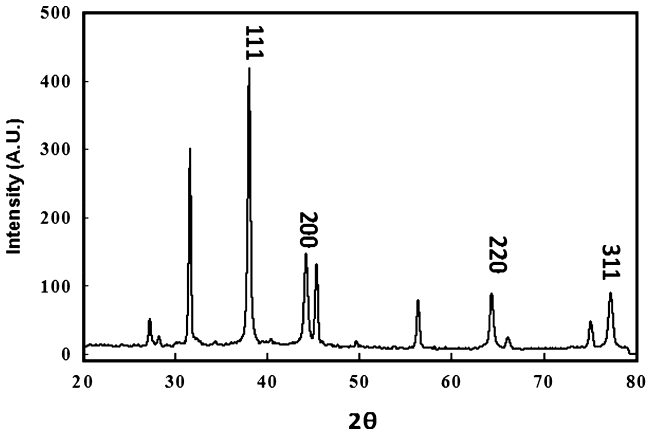

Fig. 2. XRD pattern of Rh-AgNPs. The characteristic strong diffraction peak located at 38.0° is ascribed to the (1 1 1) facets of the face-centered cubic metal silver structure.

A representative TEM image recorded for Rh-AgNPs film deposited on a carbon-coated copper grid is shown in Fig. 3(a). The image shows individual silver particles as well as some aggregates. Generally, the morphology of the Rh-AgNPs was variable but predominantly spherical NPs in the size range of 5–23 nm, which was further validated by AFM analysis. Fig. 3(b) shows the AFM image of Rh-AgNPs obtained on scanning probe microscope in tapping mode, under ambient conditions. The average size of the Rh-AgNPs and roughness (Ra) of surface were determined as 20 nm and 14 nm, respectively, using the WSXM and SPIP softwares. Furthermore, the hydrodynamic size and Zeta potential of Rh-AgNPs were also determined to be 90 nm and −42.1 mV, respectively, which suggest good dispersibility and stability.

Fig. 3(d) shows the FTIR spectra of freeze-dried powder of rhamnolipids and Rh-AgNPs. The FTIR analysis explicitly suggested the role of bacterial rhamnolipids in stabilization of AgNPs. FTIR spectrum of AgNPs showed intense absorption bands at 3422, 2925, 2855, 1736, 1655, 1459, 1379, 1124 and 1046 cm^{-1}. The absorption bands observed at 1046 cm^{-1} and 1124 cm^{-1} represent the C—O—H bending vibrations and C—O stretching vibrations due to the proteins and rhamnolipids [29], respectively. The absorption bands with wave numbers 1379 and 1459 cm^{-1} corresponds to the

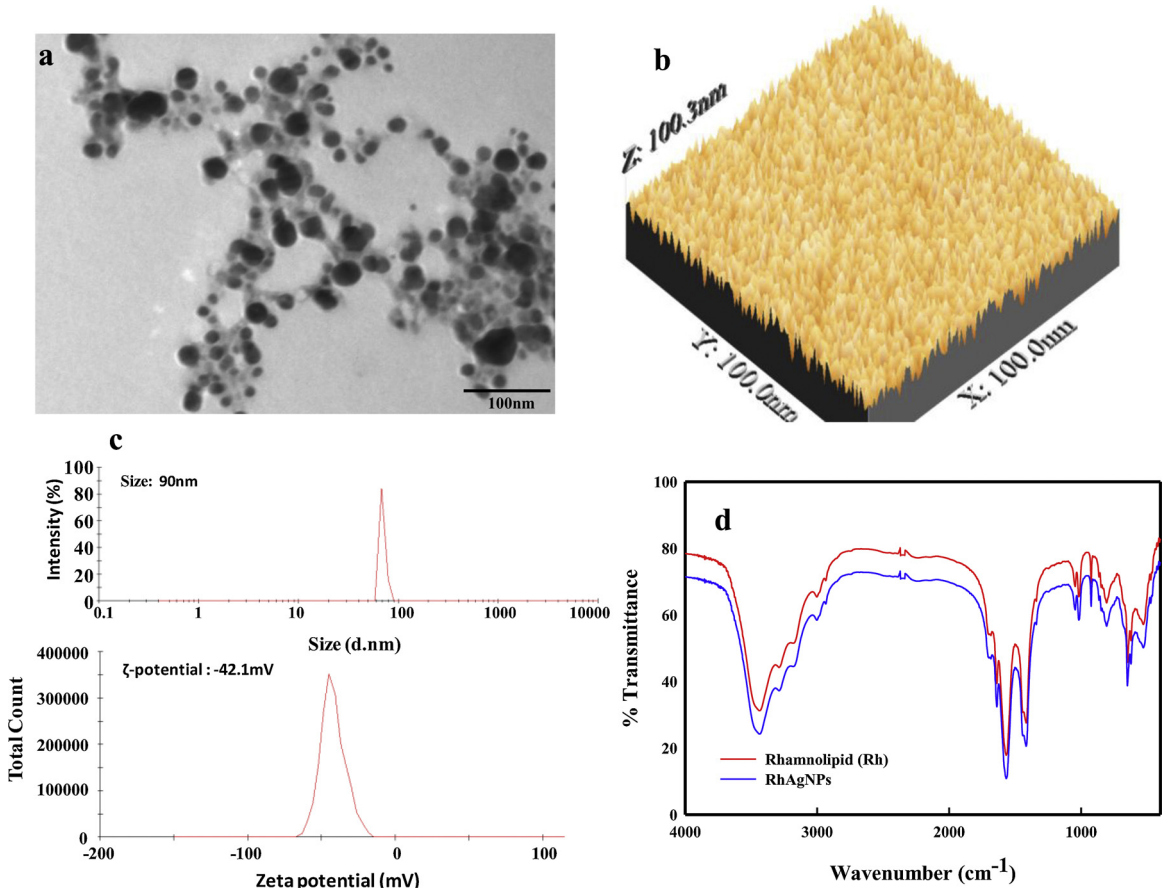

Fig. 3. Characterization of Rh-AgNPs. The panels represent: (a) TEM image of Rh-AgNPs, (b) 3D image of Rh-AgNPs analyzed by tapping mode AFM, (c) Zeta potential and hydrodynamic size of Rh-AgNPs in ultrapure water, (d) FTIR spectrum of rhamnolipid alone and Rh-AgNPs.

bending vibrations of C—H groups of rhamnolipids. The absorption band observed at wave number 1655 cm^{-1} was identified as amide-I band, which could be due to carbonyl stretch vibrations in the amide linkages of proteins [29]. The absorption band at 1736 cm^{-1} is characteristic of the C—O stretching mode of rhamnolipids [30], and the band around 3422 cm^{-1} is attributed to the N—H stretch vibrations of the peptide linkages [30], and hydroxyl stretch vibrations of the carboxylic acid group of rhamnolipids [30]. Thus, our FTIR results on Rh-AgNPs support the earlier data on purified rhamnolipids from *P. aeruginosa* strain BS-161R [30]. FTIR spectral analyses revealed subtle variations in biological components of the culture supernatant associated with the formation of AgNPs. The changes in FTIR spectra substantiated the role of rhamnolipids, as a capping agent, providing stability to Rh-AgNPs.

3.3. Rh-AgNPs induced cytotoxicity

Cultured MCF-7 cells exposed to Rh-AgNPs in concentration range of 0.5–10 μg/mL for 24 h exhibited cytotoxicity, as measured by MTT and NRU assays (Supplementary Fig. 2). The Rh-AgNPs dose dependent decrease in the cell viability is shown in Fig. 4. In MTT assay, the cell viability undergoes significant ($p < 0.05$) reduction of 82%, 78%, 73% and 29% at 1, 2, 5 and 10 μg/mL, respectively (Fig. 4A). The NRU assay also exhibited a similar trend and was found consistent with MTT data (Fig. 4B). Comparative cytotoxicity data with free Rh and Rh-AgNPs on cultured MCF-7 and normal PBMN cells at concentration of 10 μg/mL exhibited no significant effect of free Rh or Rh-AgNPs on viability of normal PBMN cells, as compared to a remarkable decrease in viability MCF-7 cells treated with Rh-AgNPs under identical concentrations (Supplementary Fig. 3). This difference in cell viability of normal verses cancer cells is attributed to the greater endocytosis activity of cancer cells than the normal cells [31–33]. Due to more negatively charged group on the surface of cancer cells, there may be a greater attachment of anionic NPs onto the MCF-7 cell plasma membrane, which promotes NPs internalization due to vesicular transport mediated cell endocytosis. Jiang et al. [34] demonstrated attenuated cytotoxicity of rhamnolipids in cell cultures in presence of 5% FBS, which could be due to inhibited surface activity. Jiang et al. [34] also suggested that previous claims on antitumor activity of rhamnolipids have been incorrectly made due to flaw in experimental design where cancer cells were either cultured in serum-free medium while normal cells were cultured in serum containing medium [35] or different exposure times to different cells were followed [36]. Thus, our results exhibiting Rh-AgNPs induced decrease in viability of MCF-7 cells with no significant effect on normal PBMN cells corroborate the earlier reported studies.

Supplementary Figs. 2 and 3 related to this article can be found, in the online version, at http://dx.doi.org/10.1016/j.colsurfb.2015.05.034

There are several drugs being prescribed for breast cancer treatment including doxorubicin, daunorubicin, bleomycin, and cisplatin [37]. However, they are expensive and known to induce cytotoxic effects in normal tissue/cells and cause other side effects such as myelosuppression, anemia, and most importantly the generation of cellular resistance [37]. Thus, our results, exhibiting dose dependent killing of MCF-7 breast cancer cells, without affecting the viability of normal PBMN cells suggest Rh-AgNPs as a suitable

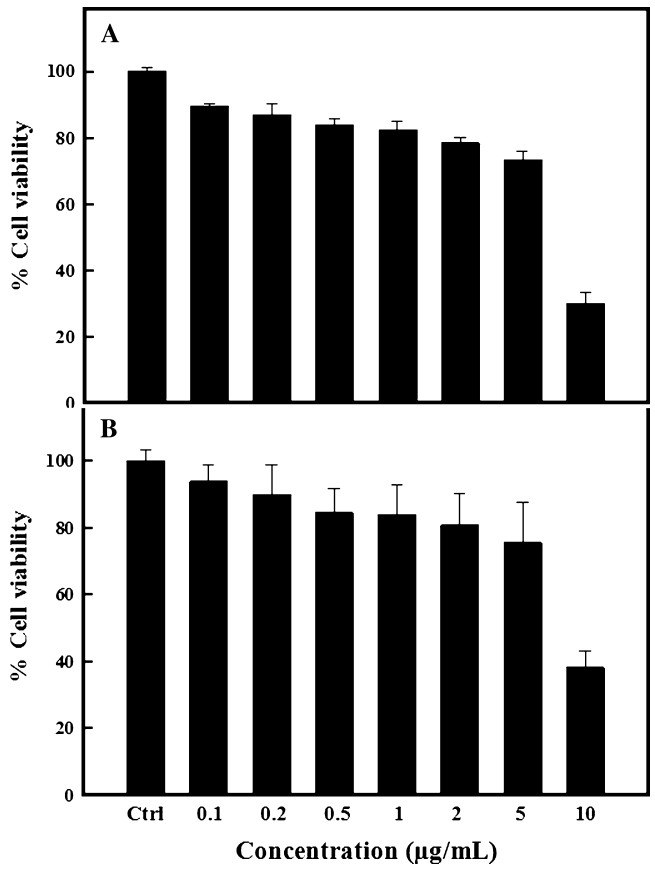

Fig. 4. (A) Rh-AgNPs induced alteration in mitochondrial activity in MCF-7 cells by MTT assay. (B) Rh-AgNPs induced alteration in the lysosomal activity in MCF-7 cells by Neutral Red Uptake assay. The values are presented as percent cell viability. Each histogram represents the values of mean ± SD of two independent experiments done in triplicate ($n = 6$). $^{*}p < 0.05$ and $^{**}p < 0.01$ vs. control.

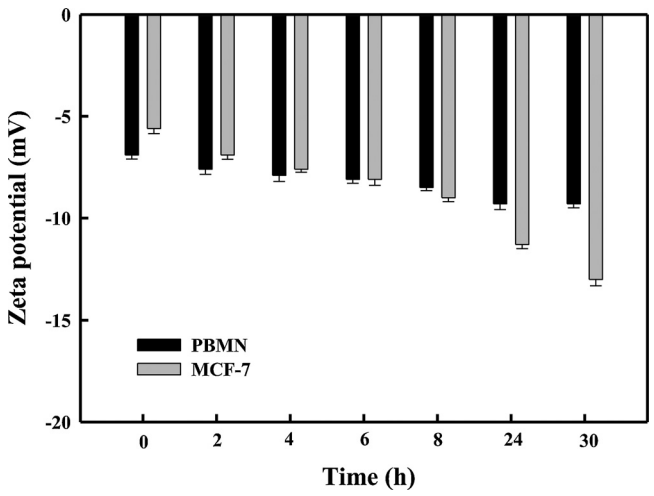

Fig. 5. Bar graphs of the Zeta potential measurement for Rh-AgNPs treated MCF-7 cancer cells and normal lymphocytes (PBMN) as control. Each histogram represents the values of mean ± SD of two independent experiments done in triplicate ($n = 6$). $^{*}p < 0.05$ and $^{**}p < 0.01$ vs. control.

alternative, to overcome these limitations. Besides, our findings also support the earlier observations on cytotoxic effects of colloidal silver on MCF-7 cells and its importance in cancer therapy [38].

3.4. Change in Zeta potential of MCF-7 cells

Fig. 5 shows the Zeta potential measurements at pH 7.4 for untreated and Rh-AgNPs treated MCF-7 cells, PBMN cells and Rh-AgNPs alone, after incubated for 24 h at 37 °C. The results demonstrated an increase in the Zeta potential (−8.16 mV to −6.0 mV) in case of Rh-AgNPs treated PBMN cells. However, the Zeta potential of treated MCF-7 cells dropped significantly from −7.32 mV to −11.17 mV. The Zeta potential of Rh-AgNPs alone has been determined to be −42.1 mV, whereas the values of control untreated PBMN and MCF-7 cells were determined to be −8.16 mV and −7.32 mV, respectively. Such a difference in surface electro kinetic properties between normal and transformed cancer cells has also been reported earlier [39]. Observed changes in Zeta potential of Rh-AgNPs treated normal and cancer cells could be due to the differential binding of charged NPs to the cell surface plasma membrane. Zeta potential has been used to diagnose the cellular interaction with charged ions or molecules. The negatively charged ions or molecules decrease the surface Zeta potential and positively charged ions increase the surface Zeta potential [40]. Indeed, more negatively charged group on the surface of cancer cells generate more negative charge of cancer cell than normal cells, which are mainly driving from the sialic acid residues protruding from the apical surface of the plasma membrane [41]. It is likely the greater attachment of anionic NPs on to the MCF-7 cell plasma membrane turns the Zeta potential more negative, which consequently promotes NPs internalization due to vesicular transport mediated cell endocytosis [42]. Thus, the difference in the ingestion activity of Rh-AgNPs between normal PBMN and MCF-7 cells leads to a greater inhibition of cancer cell proliferation than that of normal cells.

3.5. Change in mitochondrial membrane potential and ROS induced cell death in MCF-7 cells

Flow cytometry data indicated the Rh-AgNPs concentration dependent decrease in the fluorescence intensity of Rh123 stained MCF-7 cells. The treated MCF-7 cells exhibited 30.1% and 33.5% reduction in fluorescence intensity of Rh123 at 0.25 and 0.5 μg/mL Rh-AgNPs respectively (Fig. 6A). However, at concentration of 1 μg/mL, the relative fluorescence intensity decreased to 25%. The observed shift in Log FL1 peak and change in fluorescence of the dye Rh123 in Rh-AgNPs treatment MCF-7 cells explicitly suggests alteration of the inner mitochondrial membrane, and consequent mitochondrial dysfunction [43]. Fig. 6B demonstrate the Rh-AgNPs induced intracellular ROS generation in MCF-7 cells using fluorescence probe DCFH-DA through flow cytometry. A significant increase of 1.25-fold ($p < 0.05$) in the DCF fluorescence has been recorded at the lowest concentration of 0.25 μg/mL (Fig. 6B). Further exposure of MCF-7 cells to higher concentrations (0.5 and 1.0 μg/mL) of Rh-AgNPs resulted in lesser DCF fluorescence, which is again attributed to cellular lethality of Rh-AgNPs at these concentrations. Indeed, the compromised antioxidizing ability of Rh-AgNPs exposed cells, and incessant intracellular ROS generation may lead to oxidative stress [38]. The initial increase in ROS production at 0.25 μg/mL Rh-AgNPs induces the mitochondrial and DNA damage. However, the decrease in MnXI values of ROS at greater concentrations is ascribed to cellular necrosis, possibly due to disruption of plasma membrane. These observations corroborate well with our earlier results on toxicity of NPs and insecticides, where DCF fluorescence intensity has been reportedly increased initially at lower doses and then decreased at higher concentrations due to significant cell death (necrosis) [43]. Earlier studies with the colloidal silver also suggested that the decreased levels of $NADH/NAD^{+}$ in MCF-7 cells, induces cell death due to decreased mitochondrial membrane potential [38].

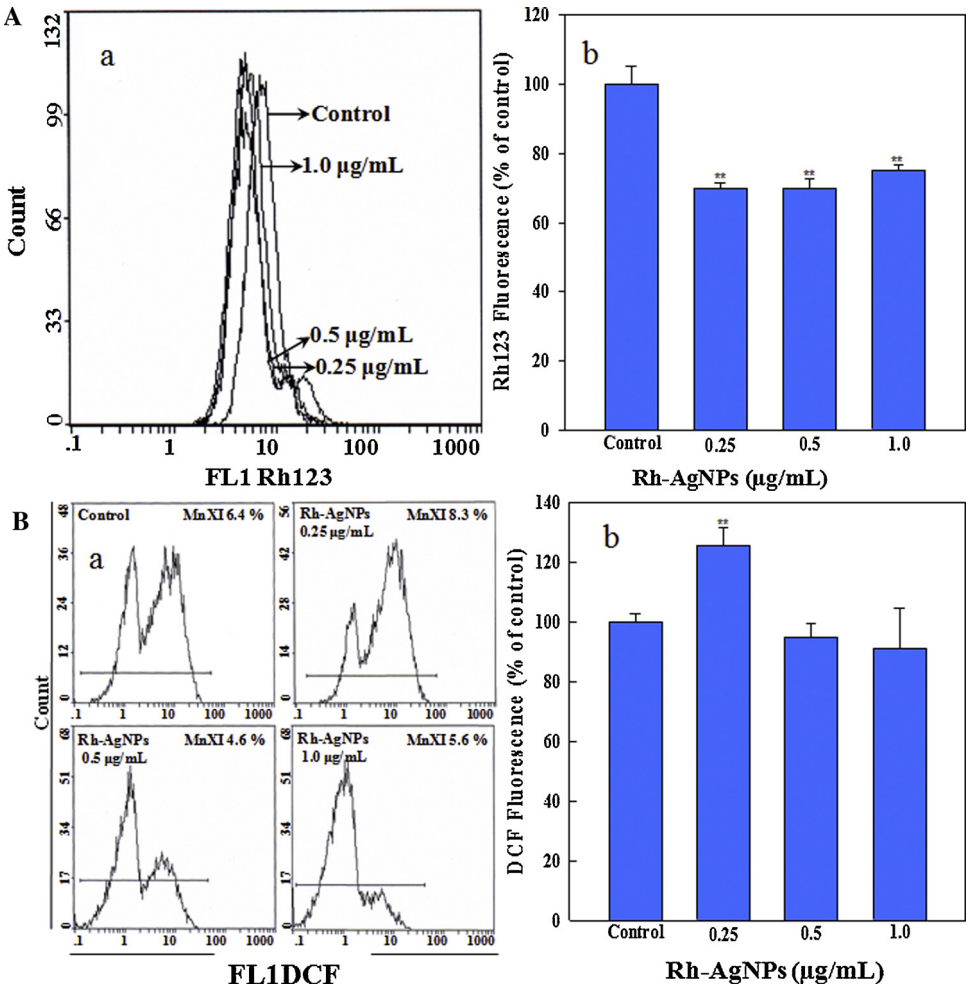

Fig. 6. Effect of Rh-AgNPs on ΔΨm and intracellular ROS generation of MCF-7 cells measured in-terms of change in the fluorescence intensity of Rh123 and DCF after 3 h. (A) (panels a–b) The flow cytometric measurements of ΔΨm in MCF-7 cells at different time periods after exposure with increasing concentrations of Rh-AgNPs. (B) (panels a–b) The concentration dependent enhancement in green fluorescence of DCF that occurs in MCF-7 cells due to ROS generation by Rh-AgNPs exposure for 3 h. Each histogram represents the values of mean ± SD of three independent experiments. $^{*}p < 0.05$ and $^{**}p < 0.01$ vs. control.

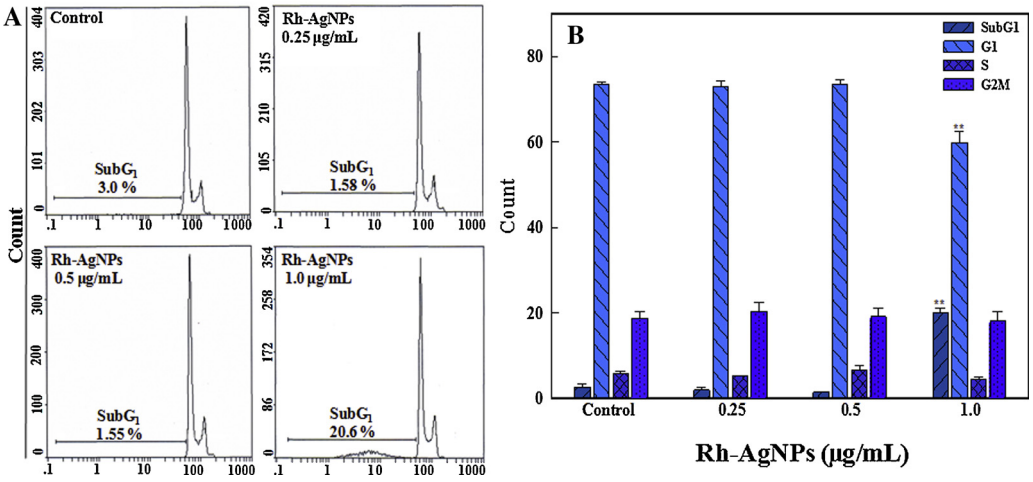

Fig. 7. Cell cycle analysis of PI-stained nuclei of MCF-7 cells. (A) Representative FACS images showing the changes in the progression of the normal cell cycle as a function of the Rh-AgNPs concentration. G1, S, G 2/M in each micrograph represent the percentage of cells present in normal phases of cell cycle, whereas SubG1, represents the percentage of cells that underwent apoptosis/necrosis, (B) Each histogram represents the mean ± SD from three independent experiments. $^{*}p < 0.05$ and $^{**}p < 0.01$ compared with the control, as determined by one-way ANOVA.

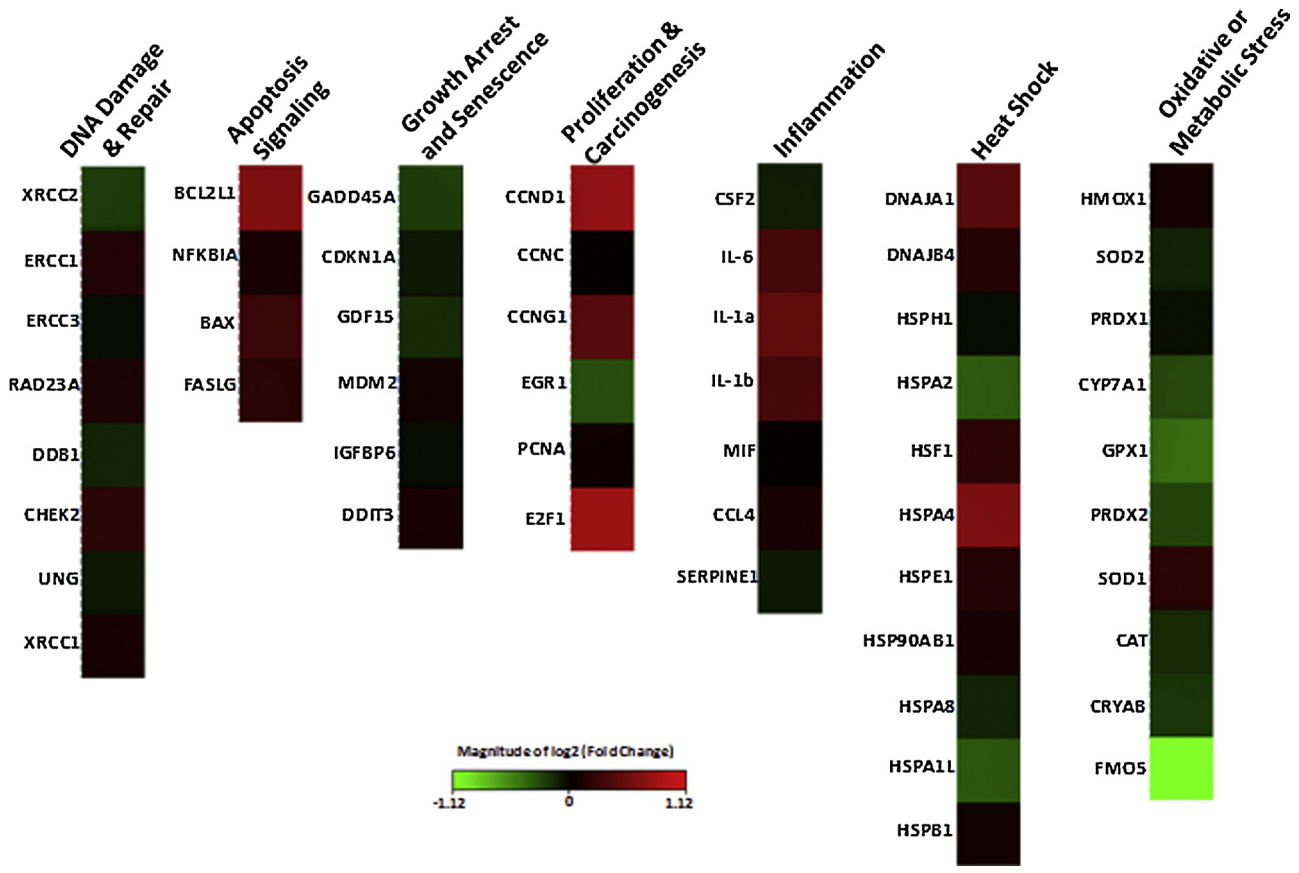

Fig. 8. qPCR array of oxidative stress and toxicity pathway genes in MCF-7 cells. Relative gene expression of 84 genes responsible for human stress and toxicity pathway in Rh-AgNPs.

3.6. Rh-AgNPs induced cell death (late apoptosis/necrosis) in MCF-7 cells

Flow cytometry data on cell cycle analysis of untreated and Rh-AgNPs treated PI-stained cells exhibited an increase in subG1 peak with concomitant reduction in G1 phase (Fig. 7). A significant increase (19.9%, $p < 0.05$) in the population of dead cells in subG1 phase has been recorded at 1 μg/mL of Rh-AgNPs, as compared to 2.7% in untreated control. No significant change in the cell cycle of MCF-7 cells has been observed at lower (0.25 and 0.5 μg/mL) concentration of Rh-AgNPs. This study demonstrated that the Rh-AgNPs have a capacity of inducing intracellular ROS, which eventually triggers the development of mitochondrial membrane damage leading to cell cycle alterations and necrosis, indicative of Rh-AgNPs anticancer potential in exposed human MCF-7 cells.

3.7. Rh-AgNPs induced gene expression in MCF-7 cells

Pathway-focused gene expression heat maps shown in Fig. 8 exhibited both the down regulation and upregulation of certain mRNA transcripts in the range of −1.12 to +1.12, respectively. The upregulated genes were identified as BCl_2 (1.53 fold), Cyclin D1 (1.65 fold), DNAJA1 (1.33 fold), E2F transcription factor 1 (1.66 fold), GPX1 (1.32 fold) and HSPA4 (1.49 fold) (Fig. 8). However, some genes from the DNA damage and repair pathway (XRCC2, DDB1), growth and senescence (GADD45A, GDF15, IGFBP6), proliferation and carcinogenesis (EGR1), heat shock proteins (HSP2, HSPA1L) and oxidative or metabolic stress pathways (CYP7A1, GPX1, PRDX2, CAT, CRYAB, and FMO5) were negatively down regulated (Fig. 8). The data revealed the upregulation of the genes involved in apoptosis signaling, proliferation and carcinogenesis, pro inflammatory and heat shock responses in cell treated with Rh-AgNPs. The down regulation of gene in oxidative stress pathway may disrupt the redox balance in cells and promote cellular damage as manifested in terms of mitochondrial membrane damage and dissipation of membrane potential. The BCl_2 and cyclin D1 genes stimulate apoptotic pathway, as also evident with our flow cytometry data on cell cycle inhibition. In conclusion, the antiproliferative activity of Rh-AgNPs against the MCF-7 cancer cells is possibly due to their attachment of NPs to the surface of the cell, leading to disruption of cell membrane and oxidative stress, which suggest the role of Rh-AgNPs as a promising candidate for biomedical and clinical applications.

Conflict of interest

There is no conflict of interest.

Acknowledgments

The Chair for DNA research, King Saud University, Riyadh, for this study, is greatly acknowledged. JM is also grateful to the Visiting Professor Program (VPP), King Saud University for all support to carry out this collaborative research.

References

[1] M. Merroun, A. Rossberg, C. Hennig, A.C. Scheinost, S. Selenska-Pobell, Spectroscopic characterization of gold nanoparticles formed by cells and S-layer proteins of *Bacillus sphaericus* JG-A12, Mater. Sci. Eng. 27 (2007) 188–192.

[2] M. Valodkar, A. Bhadoria, J. Pohnerkar, M. Mohan, S. Thakore, Morphology and antibacterial activity of carbohydrate-stabilized silver nanoparticles, Carbohydr. Res. 345 (2010) 1767–1773.
[3] S. Jaiswal, B. Duffy, A.K. Jaiswal, N. Stobie, P. McHale, Enhancement of the antibacterial properties of silver nanoparticles using beta-cyclodextrin as a capping agent, Int. J. Antimicrob. Agents 36 (2013) 280–283.
[4] D. Wei, W. Sun, W. Qian, Y. Ye, X. Ma, The synthesis of chitosan-based silver nanoparticles and their antibacterial activity, Carbohydr. Res. 344 (2009) 2375–2382.
[5] J. Musarrat, S. Dwivedi, B.R. Singh, A.A. Al-Khedhairy, A. Azam, A. Naqvi, Production of antimicrobial silver nanoparticles in water extracts of the fungus *Amylomyces rouxii* strain KSU-09, Bioresour. Technol. 101 (2010) 8772–8776.
[6] S. Dwivedi, A.A. Alkhedhairy, M. Ahamed, J. Musarrat, Biomimetic synthesis of selenium nanospheres by bacterial strain JS-11 and its role as a biosensor for nanotoxicity assessment: a novel se-bioassay, PLoS ONE 8 (2013) e57404.
[7] A.M. Fayaz, K. Balaji, M. Girilal, R. Yadav, P.T. Kalaichelvan, R. Venketesan, Biogenic synthesis of silver nanoparticles and their synergistic effect with antibiotics: a study against Gram-positive and Gram-negative bacteria, Nanomedicine 6 (2010) 103–109.
[8] S. Anil Kumar, K.A. Majid, S.W. Gosavi, S.K. Kulkarni, R. Pasricha, A. Ahmad, M.I. Khan, Nitrate reductase mediated synthesis of silver nanoparticles from $AgNO_3$, Biotechnol. Lett. 29 (2007) 439–445.
[9] P. Mukherjee, A. Ahmad, D. Mandal, S. Senapati, S.R. Sainkar, M.I. Khan, R. Parischa, P.V. Ajaykumar, M. Alam, R. Kumar, M. Sastry, Fungus mediated synthesis of silver nanoparticles and their immobilization in the mycelial matrix: a novel biological approach to nanoparticle synthesis, Nano Lett. 1 (2001) 515–519.
[10] A. Ahmad, P. Mukherjee, S. Senapati, D. Mandal, M.I. Khan, R. Kumar, M. Sastry, Extracellular biosynthesis of silver nanoparticles using the fungus *Fusarium oxysporum*, Colloids Surf. B: Biointerfaces 28 (2003) 313–318.
[11] A.S. Malik, M.J. Duncan, P.G. Bruce, Mesostructured iron and manganese oxides, J. Mater. Chem. 13 (2003) 2123–2126.
[12] Z.Y. Yuan, T.Z. Ren, B.L. Su, Surfactant-mediated nanoparticle assembly of catalytic mesoporous crystalline iron oxide materials, Catal. Today 93–95 (2004) 743–750.
[13] H. Ghojavand, F. Vahabzadeh, M. Mehranian, M. Radmehr, A. ShahrakiKh, F. Zolfagharian, M.A. Emadi, E. Roayaei, Isolation of thermo tolerant, halotolerant, facultative biosurfactant-producing bacteria, Appl. Microbiol. Biotechnol. 80 (2008) 1073–1085.
[14] S. Mukherje, P. Das, R. Sen, A review of towards commercial production of microbial surfactants, Trends Biotechnol. 24 (2006) 509–515.
[15] C.G. Kumar, S.K. Mamidyala, B. Das, B. Sridhar, G.S. Devi, M.S. Karuna, Synthesis of biosurfactant based silver nanoparticles with purified rhamnolipids isolated from *Pseudomonas aeruginosa* BS-161R, J. Microbiol. Biotechnol. 20 (2010), 1061-8.M.
[16] Y. Xie, R. Ye, H. Liu, Synthesis of silver nanoparticles in reverse micelles stabilized by natural biosurfactant, Colloids Surf. A – Physicochem. Eng. Asp. 279 (2006) 175–178.
[17] M. Robert, M.E. Mercade, M.P. Bosch, J.L. Parra, M.J. Espuny, M.A. Manresa, J. Guinea, Effect of the carbon source on biosurfactant production by *Pseudomonas aeruginosa* 44Ti, Biotechnol. Lett. 11 (1989) 871–874.
[18] M.E. Mercade, M.A. Manresa, M. Robert, M.J. Espuny, C. deAndres, J. Guinea, Olive oil mill effluent (OOME) new substrate for biosurfactant production, Bioresour. Technol. 43 (1993) 1–6.
[19] S. Dwivedi, B.R. Singh, A.A. Al-Khedhairy, J. Musarrat, Biodegradation of isoproturon using a novel *Pseudomonas aeruginosa* strain JS-11 as a multi-functional bioinoculant of environmental significance, J. Hazard. Mater. 185 (2011) 938–944.
[20] S. Inka, W. Fritz, New method for detecting rhamnolipids excreted by *Pseudomonas* species during growth on mineral agar, Biotechnol. Tech. 5 (1991) 265–268.
[21] J.D. Sheppard, C.N. Mulligan, The production of surfactin by *Bacillus subtilis* grown on peat hydrolysate, Appl. Microbiol. Biotechnol. 27 (1987) 110–116.
[22] A.L. Patterson, The Scherrer formula for X-ray particle size determination, Phys. Rev. 699 (1939) 978–982.
[23] J.P. Saikia, P. Bharali, B.K. Konwar, Possible protection of silver nanoparticles against salt by using rhamnolipid, Colloids Surf. B: Biointerfaces 104 (2013) 330–332.
[24] J. Musarrat, Q. Saquib, A. Azam, S.A.H. Naqvi, Zinc oxide nanoparticles-induced DNA damage in human lymphocytes, Int. J. Nanoparticles 2 (2009) 402–415.
[25] S. Dwivedi, M.A. Siddiqui, N.N. Farshori, M. Ahamed, J. Musarrat, A.A. Al-Khedhairy, Synthesis characterization and toxicological evaluation of iron oxide nanoparticles in human lung alveolar epithelial cells, Colloids Surf. B: Biointerfaces 122C (2014) 209–215.
[26] M.A. Siddiqui, H.A. Alhadlaq, J. Ahmad, A.A. Al-Khedhairy, J. Musarrat, M. Ahamed, Copper oxide nanoparticles induced mitochondria mediated apoptosis in human hepatocarcinoma cells, PLoS ONE 8 (2013) e69534.
[27] K.S.M.P. Rahman, P. Godfrey, A. Vincent, A. Zulf, Production of rhamnolipid Biosurfactants by *Pseudomonas aeruginosa* DS10-129 in a microfluidic bioreactor, Biotechnol. Appl. Biochem. 55 (2010) 45–52.
[28] W. Kleemann, Random-field induced antiferromagnetic, ferroelectric and structural domain states, Int. J. Mod. Phys. B 7 (1993) 2469–2507.
[29] C.G. Kumar, S.K. Mamidyala, Extracellular synthesis of silver nanoparticles using culture supernatant of *Pseudomonas aeruginosa*, Colloids Surf. B: Biointerfaces 1 (2011) 462–466.
[30] C.G. Kumar, S.K. Mamidyala, B. Das, B. Sridhar, G.S. Devi, M.S. Karuna, Synthesis of biosurfactant-based silver nanoparticles with purified rhamnolipids isolated from *Pseudomonas aeruginosa* BS-161R, J. Microbiol. Biotechnol. 20 (2010) 1061–1068.
[31] M.B. Omary, I.S. Trowbridge, J. Minowada, Human cell-surface glycoprotein with unusual properties, Nature 286 (1980) 888–891.
[32] R. Sutherland, D. Delia, C. Schneider, R. Newman, J. Kemshead, M. Greaves, Ubiquitous cell-surface glycoprotein on tumor cells is proliferation-associated receptor for transferring, Proc. Natl. Acad. Sci. 78 (1981) 4515–4519.
[33] T.R. Daniels, T. Delgado, J.A. Rodriguez, G. Helguera, M.L. Penichet, The transferrin receptor part I: biology and targeting with cytotoxic antibodies for the treatment of cancer, Clin. Immunol. 121 (2006) 144–158.
[34] L. Jiang, C. Shen, X. Long, G. Zhang, Q. Meng, Rhamnolipids elicit the same cytotoxic sensitivity between cancer cell and normal cell by reducing surface tension of culture medium, Appl. Microbiol. Biotechnol. 98 (2014) 10187–10196.
[35] B. Thanomsub, W. Pumeechockchai, A. Limtrakul, P. Arunrattiyakorn, W. Petchleelaha, T. Nitoda, H. Kanzaki, Chemical structures and biological activities of rhamnolipids roduced by *Pseudomonas aeruginosa* B189 isolated from milk factory waste, Bioresour. Technol. 97 (2006) 2457–2461.
[36] N. Christova, B. Tuleva, A. Kril, M. Georgieva, S. Konstantinov, I. Terziyski, B. Nikolova, I. Stoineva, Chemical structure and in vitro antitumor activity of rhamnolipids from *Pseudomonas aeruginosa* BN10, Appl. Biochem. Biotechnol. 170 (2013) 676–689.
[37] D.W. Kim, G.H. Hong, H.H. Lee, S.H. Choi, B.G. Chun, C.K. Won, I.K. Hwang, M.H. Won, Effect of colloidal silver against the cytotoxicity of hydrogen peroxide and naphthazarin on primary cultured cortical astrocytes, Int. J. Neurosci. 117 (2007) 387–400.
[38] M.A. Franco-Molina, E. Mendoza-Gamboa, C.A. Sierra-Rivera, R.A. Gómez-Flores, P. Zapata-Benavides, P. Castillo-Tello, J.M. Alcocer-Gonzalez, D.F. Miranda-Hernández, R.S. Tamez-Guerra, C. Rodríguez-Padilla, Antitumor activity of colloidal silver on MCF-7 human breast cancer cells, J. Exp. Clin. Cancer Res. 29 (2010) 148.
[39] G.M.W. Cook, W. Jacobson, The electrophoresis mobility of normal and leukaemic cells of mice, Biochem. J. 107 (1968) 549–550.
[40] F.C. Silva Filho, A.B. Santos, T.M. de Carvalho, W. de Souza, Surface charge of resident, elicited, and activated mouse peritoneal macrophages, J. Leukoc. Biol. 41 (1987) 143–149.
[41] Y. Han, S. Li, X. Cao, L. Yuan, Y. Wang, Y. Yin, T. Qiu, H. Dai, X. Wang, Different inhibitory effect and mechanism of hydroxyapatite nanoparticles on normal cells and cancer cells, in vitro and in vivo, Sci. Rep. 4 (2014) 7134.
[42] G.M. Cooper, The Cell: A Molecular Approach, 2nd edn., ASM Press, Washington D.C., 2000.
[43] S. Dwivedi, Q. Saquib, A.A. Al-Khedhairy, J. Musarrat, Butachlor induced dissipation of mitochondrial membrane potential, oxidative DNA damage and necrosis in human peripheral blood mononuclear cells, Toxicology 302 (2012) 77–87.